DOI: 10.1002/fuce.201600024

Fuel Cells

ORIGINAL RESEARCH PAPER

Simulation of Proton Transport in Proton Exchange Membranes with Reactive Molecular Dynamics▲

C. Arntsen[1], J. Savage[1], Y.-L. S. Tse[1,2], G. A. Voth[1]*

[1] Department of Chemistry, The James Franck Institute, and Computation Institute, University of Chicago, Chicago, IL 60637, USA
[2] Department of Chemistry, The Chinese University of Hong Kong, Shatin, New Territories, Hong Kong, China

Received February 11, 2016; accepted March 08, 2016; published online April 04, 2016

Abstract

Proton exchange membrane fuel cells (PEMFCs) are promising to become the next generation of energy conversion devices that are efficient, lightweight, and have clean emissions. In these cells, a hydrated polymer membrane acts as an electrolyte layer through which protons travel. Due to the complex nature of the membranes used, the optimization of fuel cell performance is a difficult task, and relies on a number of factors, such as hydration level, polymer side chain length and composition, equivalent weight, morphology, and chemical and mechanical stabilities. Molecular dynamics is a particularly powerful tool for studying PEMs, as it provides the computational efficiency to study length and time scales relevant to these systems. In this review, we present results from several computational papers that use reactive molecular dynamics, which explicitly describe bond breaking and formation, to study proton transport in several polymers commonly used in PEMs. The results presented demonstrate the importance of the interaction between hydronium and the charged side chains and the morphology on the performance of PEM fuel cells.

Keywords: Molecular Dynamics, Morphological Effects, Perfluorosulfonic Acid Membranes, Proton Exchange Membrane, Proton Transport

1 Introduction

With an increase in concern over the impacts of climate change, renewable and clean energy sources are gaining attention as alternatives to fossil fuels. Proton exchange membrane fuel cells (PEMFCs) in particular are a promising energy technology with a wide array of potential applications [1], and have received considerable attention in both experimental [2–14] and computational studies [15–61]. PEMFCs are particularly attractive in that they are efficient, lightweight, and have clean emissions. In PEMFCs, a hydrated polymer membrane acts as an electrolyte, allowing for efficient proton transport to the cathode of the fuel cell, and as a barrier to keep gaseous fuels separate. The most common polymers used in PEMs are perfluorosulfonic acid (PFSA) polymers, which consist of a polytetrafluoroethylene backbone and sulfonated side chains. Nafion [62] has long been the champion polymer in PEMFCs, though other similar PFSA membranes have since surpassed it in terms of performance [63, 64].

There are numerous factors determining the conductivity of a given polymer in a PEM, including crystallinity, equivalent weight [63], hydration level [36, 47, 56], side chain length [30, 36, 65–67], and morphology [61, 68]. Due to the vast parameter space offered by the diverse set of conditions, optimizing the performance of PEMs can be a highly complex and time-consuming process. While conditions in experiments can be difficult to control, computer simulations allow one to investigate the influence of individual parameters, such as hydration level or equivalent weight, and can be a useful tool for studying PEMs. However, modeling the polymer layers used in PEMFCs can be very complicated due to their amorphous nature.

Classical molecular dynamics (MD) simulations would seem an optimal choice for studying PEMs, as it can access many of the relevant length and time scales. Proton diffusion

▲ *Publication is part of the Topical Issue "Theory and Modeling of Fuel Cells" 2016.*

[*] *Corresponding author, gavoth@uchicago.edu*

largely determines the conductivity performance of a fuel cell, and it involves at least two mechanisms: vehicular transport and Grotthuss shuttling. The Grotthuss mechanism for proton transport involves the rearrangement of chemical and hydrogen bonds of hydronium and water, and a theoretical investigation into this mechanism, therefore requires the ability to capture bond breaking and formation. Traditional MD approaches cannot explicitly handle changes in the bonding topology and cannot be used to capture the essential physics and chemistry of proton transport in PEMs. *Ab initio* molecular dynamics (AIMD) naturally takes into account breaking and formation of chemical bonds, but its high cost proves prohibitively expensive when studying the length scales relevant to proton diffusion in PEMs. The work described in this paper employs the multistate empirical valence bond (MS-EVB) method [69–72], which can capture the Grotthuss mechanism and has been shown to accurately describe proton transport in PEMs [20, 21, 28, 47, 52, 55, 56, 59, 60]. In the MS-EVB framework, the bonding topology of a system is not fixed. Rather, the ground state of a system $|\Psi\rangle$ can be described by a linear combination of basis states $|i\rangle$, each of which describes a different bonding topology:

$$|\Psi\rangle = \sum_{i=1}^{N} c_i |i\rangle \tag{1}$$

where N is the number of basis states, and the c_i's are obtained by diagonalizing the EVB Hamiltonian:

$$\mathbf{Hc} = E_0 \mathbf{c} \tag{2}$$

The matrix elements of the Hamiltonian $\mathbf{H}$ in Eq. (2) are defined,

$$h_{ij} = \langle i|\mathbf{H}|j\rangle \tag{3}$$

and E_0 is the ground state energy. The eigenvector $\mathbf{c}$ is normalized such that

$$\sum_{i=1}^{N} c_i^2 = 1 \tag{4}$$

This framework allows for charge delocalization and dynamic bond rearrangement.

In this review, we discuss several computational studies which use the MS-EVB scheme to investigate the effects of water model [56], side-chain composition [60], and morphology [52] on proton dynamics and nanometer-scale structure. We first compare the results of (nonreactive) classical molecular dynamics simulations to those of (reactive) MS-EVB simulations, which highlight the importance of the Grotthuss mechanism [73] to overall proton transport in PEMs. We then compare the structural and dynamics properties of two PFSA membranes, 3M and Hyflon. Both materials have identical polytetrafluoroethylene backbones, but sulfonated side chains of differing lengths, so we can directly compare the effects of side chain length on proton self-diffusion. In doing so, we propose a transport mechanism in which protons are passed between adjacent sulfonate groups. In this mechanism, the electrostatic potential well of the sulfonate groups may be quite deep, but if the overlap of such wells is sufficiently high, protons can be efficiently transported.

We then compare the properties of Nafion with different morphologies: lamellae and water channels. The lamellar morphology consists of parallel slabs of polymer separated by water layers, the thicknesses of which are varied in the study presented here. The water channel model consists of cylindrical channels of water embedded within the polymer layer; the radius of the water channel is varied. Based on the proton transport mechanism proposed, we can draw several conclusions on how sulfonate aggregation, which is dependent on the morphology of the system, affects proton transport.

2 Results and Discussion

2.1 Importance of Reactivity in Simulating Proton Transport

The primary advantage of the MS-EVB scheme is its ability to capture both vehicular and Grotthuss mechanisms of proton transport efficiently and accurately [47, 69, 70, 72, 74, 75]. To emphasize that importance, we can compare proton self-diffusion rates of Nafion and 3M calculated using MS-EVB to two nonreactive water models: F3C [76] and SPC/Fw [77]. For the nonreactive models, the proton self-diffusion is defined by the diffusion of hydronium ions. In MS-EVB, since the excess proton is described by numerous EVB states, we define the self-diffusion by the position of the excess proton as the center of excess charge (CEC),

$$\mathbf{r}_{CEC} = \sum_{i=1}^{N} c_i^2 \mathbf{r}_{COC}^i \tag{5}$$

where $\mathbf{r}_{\mathrm{COC}}^i$ is the position of the center-of-charge of the ith EVB state. The reactive simulations use the MS-EVB 3.0 model, which was parameterized with SPC/Fw water [72]. The results showing the proton self-diffusion constants as a function of model and hydration level at 300 K and 353 K are shown in Figure 1. First, notice that under all conditions, nonreactive SPC/Fw has a slower self-diffusion constant when compared to MS-EVB, despite having the same underlying water model. This shows how important reactivity is in fully capturing proton transport in a PEM. F3C shows a similar self-diffusion constant as MS-EVB in Nafion at all hydration levels at 300 K, but a slower diffusion at 353 K. On the other hand, for 3M, F3C diffusion is slower at all hydration levels and temperatures. Figure 1 also shows the experimental diffusion constants for Nafion derived from conductivity data and from quasielastic neutron scattering (QENS) experiments [78–80]. While the reactive simulations underestimate the proton self-diffusion rates when compared to experiment, they are in better agreement than either nonreactive model.

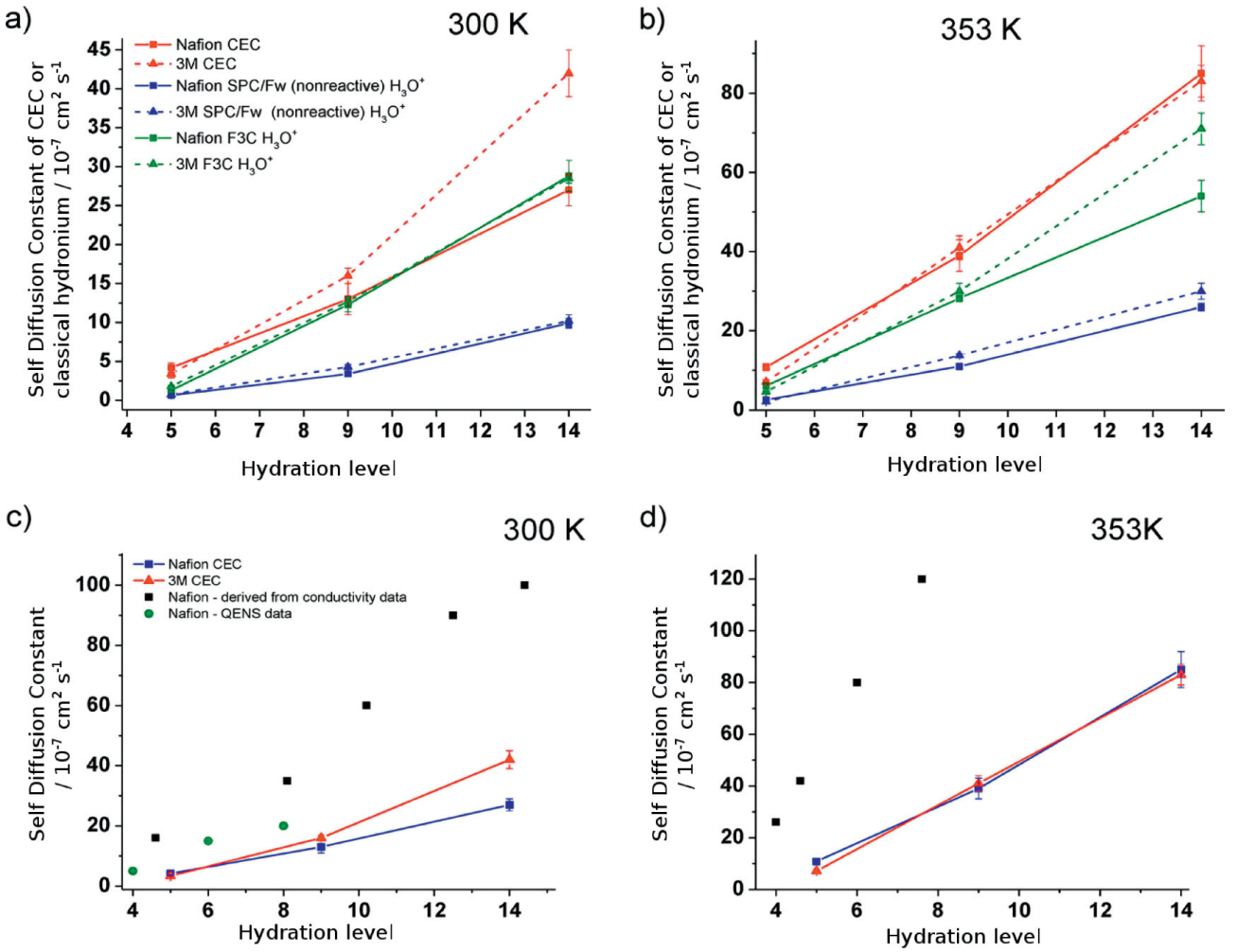

Fig. 1 Self-diffusion constant of CEC and classical hydronium of Nafion and 3M at hydration levels 5, 9, and 14 at (a) 300 K and (b) 353 K. Experimental data of Nafion alongside CEC self-diffusion constants at (c) 300 K and (d) 353 K. Reprinted with permission from Y.-L. S. Tse, A. M. Herring, K. Kim, G. A. Voth, *J. Phys. Chem. C* 2013, *117*, 8079. Copyright 2013 American Chemical Society. Experimental data from Ref. [78–80].

The difference between the reactive model and the classical models is the inclusion of the Grotthuss mechanism. It is therefore interesting to compare the influence of the hopping mechanism to the overall transport and to the contribution from vehicular transport. In order to make such a comparison, the proton displacement is decomposed into contributions from discrete hops and from continuous movement:

$$\Delta\mathbf{r}_{CEC}(t) = \Delta\mathbf{r}_C(t) + \Delta\mathbf{r}_d(t) \tag{6}$$

$$\left\langle|\Delta\mathbf{r}_{CEC}(t)|^2\right\rangle = \left\langle|\Delta\mathbf{r}_C(t)|^2\right\rangle + \left\langle|\Delta\mathbf{r}_d(t)|^2\right\rangle + 2\langle\Delta\mathbf{r}_c(t)\cdot\Delta\mathbf{r}_d(t)\rangle \tag{7}$$

where $\Delta\mathbf{r}_d(t)$ and $\Delta\mathbf{r}_c(t)$ are the discrete and continuous components of the total displacement, $\Delta\mathbf{r}_{\mathrm{CEC}}(t)$. In our decomposition, we define a discrete hop as a change in identity of the most probable hydronium EVB state over a 100 fs time interval. If the CEC has hopped in this interval, the displacement is assigned to the discrete component; otherwise it is assigned to the continuous component (see Ref. [56] for a more detailed description of how these components are separated and defined). The total mean squared displacement (MSD) as well as the discrete and continuous contributions for 3M at hydration level 14 and 300 K are shown in Figure 2. Notice that the sum of the discrete and continuous MSDs is much larger than the total MSD. This indicates that the two components are anti-correlated, i.e. the term $\langle\Delta\mathbf{r}_c(t)\cdot\Delta\mathbf{r}_d(t)\rangle$ in Eq. (7) is negative, a phenomenon not seen in a system of bulk water with an excess proton [21]. Despite this anti-correlation, we see that the overall effect of including both mechanisms contributes positively to the overall proton transport. We also find that the MSDs per discrete hop and continuous move both increase with an increase in temperature and hydration level, though the MSD per discrete hop is more sensitive than per continuous move.

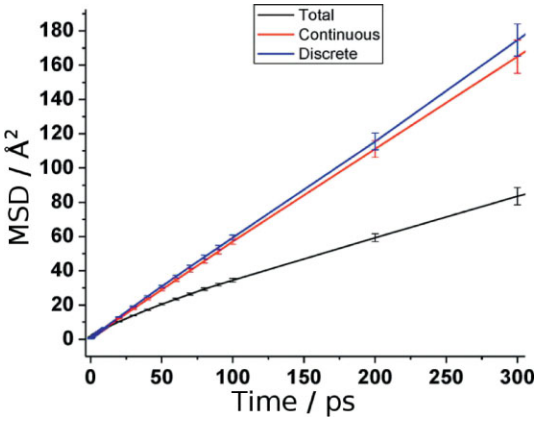

Fig. 2 MSD decomposition of 3M at hydration level 14 and 300 K. Reprinted with permission from Y.-L. S. Tse, A. M. Herring, K. Kim, G. A. Voth, *J. Phys. Chem. C* 2013, *117*, 8079. Copyright 2013 American Chemical Society.

2.2 Structure of Hydrophobic/Hydrophilic Regions

To understand the nature of proton transport in PEMs, one must examine the structure of the hydrophobic and hydrophilic domains. Figure 3 shows the connectivity of the water domains in Nafion with a random morphology at hydration level 9 and 300 K. Included in the plots are the sulfonate groups to show their location within the phase segregated system. Two important characteristics of PEMs immediately jump out. First, the aqueous layer forms a well-connected network, allowing for efficient proton transport throughout the PEM. Second, all of the sulfonates in the system accumulate at the hydrophobic-hydrophilic interface. This should not be too surprising considering that at the hydration levels studied, the sulfonate groups are completely deprotonated [18, 22, 23, 49] and carry a net charge, meaning they should have a much stronger affinity for the hydrophilic region.

Intuition would suggest that sulfonate groups sitting at the interface should reduce the proton diffusion rate, as hydronium ions in the water layer would be bound to the charged sulfonate groups by Coulombic forces, and would therefore be unable to diffuse readily throughout the system. As we demonstrate next, the Coulombic interactions between the hydronium ions and charged sulfonate groups do not lower the proton diffusion and in fact play a crucial role in the proton transport mechanism.

2.3 Solvation Structure

In order to gain insight into the proton transport mechanism, we compared the structure and diffusion behavior of 3M and Hyflon, both of which have higher self-diffusion constants than Nafion [63, 64]. Both materials, however, show higher crystallinity and have shorter side chains, allowing for a smaller equivalent weight. Therefore, in order not to conflate the influence of numerous system parameters, we directly compare the proton transport behavior of 3M and Hyflon.

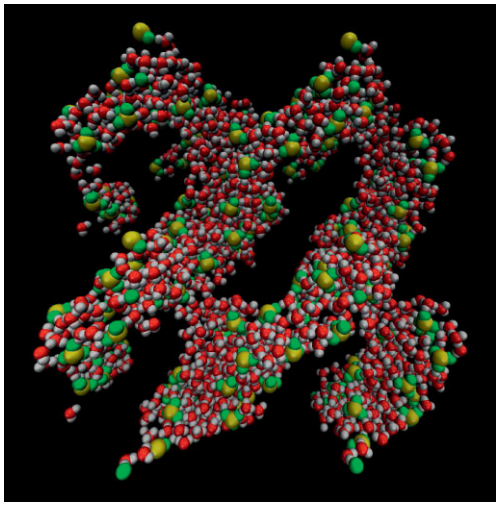

Fig. 3 Snapshot of hydrophilic domain in Nafion at hydration level 9 and 300 K. Oxygen atoms in water and hydronium are shown in red; hydrogen atoms in water and hydronium are shown in white; sulfur atoms in the sulfonate group are shown in yellow; and oxygen in the sulfonate group are shown in green; all other atoms have been omitted.

Since the two have very similar side chains, we compare the effects of side chain length at a given equivalence weight and of equivalence weight for a given side chain. The systems studied in this section are 3M with an equivalent weight of 825 (labeled "825 EW 3M"), and Hyflon with equivalent weights of 850 and 1,100 (labeled "850 EW Hyflon" and "1100 EW Hyflon" respectively) [60].

One might infer that Hyflon ought to have a faster proton diffusion constant since the shorter side chain would extend less into the aqueous pore, and the charged sulfonate groups would have weaker Coulombic interactions with hydronium ions. Figure 4 shows that this is not the case: longer chain 3M in fact has a larger proton diffusion constant.

Another important takeaway from Figure 4 is the influence on the Lennard-Jones (LJ) interactions between hydronium hydrogens and sulfonate oxygens. Previous work on PEMs had used the standard Lorentz-Berthelot mixing rules for all LJ interactions, though it was later found that this results in an over-

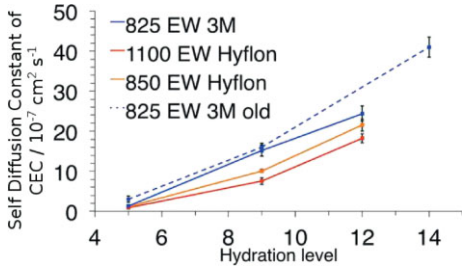

Fig. 4 Self-diffusion constants of 3M and Hyflon at hydration levels 5, 9, and 12. Self-diffusion constants of 3M without addition hydronium hydrogen – sulfonate oxygen LJ repulsion is also shown, labeled ''825 EW 3M old''. Reprinted with permission from J. Savage, Y.-L. S. Tse, G. A. Voth, *J. Phys. Chem. C* 2014, *118*, 17436. Copyright 2014 American Chemical Society.

binding of the hydronium ion to the sulfonate group. In order to dampen this attraction, the LJ potential between hydronium hydrogen and sulfonate oxygen was re-fit to match the $O_{sulfonate} - O_{hydronium}$ *ab initio* RDF (see Ref. [60] for more details on this modification). Figure 4 shows that for 3M, this modified LJ term does not have a substantial impact on calculated diffusion constants. This is particularly surprising considering the 3M systems without the added repulsive terms show a significantly pronounced peak in the $S_{sulfonate} - O_{hydronium}$ RDF below 4.5 Å, indicating that in such systems, the hydronium ion is far more likely to be in the first solvation shell of the sulfonate group. This, too, contradicts intuition, as one would expect an increase in residence time in the first solvation shell of the sulfonate group – particularly considering the electrostatic attraction of the two charged groups – would diminish proton mobility, and Figure 4 shows this does not occur.

The proton diffusion can be decomposed into two distinct components: diffusion in which a proton is associated with a sulfonate group, and diffusion in which a proton is free from all sulfonate groups. In the results presented, a proton is considered to be associated with a sulfonate group if it is within 4.5 Å of the sulfur (see Ref. [60] for a more detailed explanation of the decomposition of the displacement into respective components). The MSDs of free and associated protons for 3M and Hyflon are shown in Figure 5. As the plots show, the displacement of protons within the first solvation shell contributes quite significantly to the overall displacement. This strongly contradicts the notion that the majority of proton diffusion occurs in the center of the water pore.

To understand the increase in displacement, one must consider the spatial arrangement of the sulfonate groups. In 3M, the first solvation shells of sulfurs overlap more extensively than in Hyflon. Coupled with the observation that protons can be within the first solvation shell of more than one sulfonate group (and are quite likely to be within the second solvation shell of several sulfonate groups), the proximity of sulfonate groups indicates that protons are not trapped within the electrostatic potential well of a single sulfonate group, but are in fact able to move between them. That is, while the electrostatic well for the hydroniums may be deep, with sufficient overlap, a proton can readily move between wells. The enhancement of overlap in 3M relative to Hyflon is a function of the relative flexibility of that side chain. Due to its longer length, 3M extends farther into the hydrophilic region and can assume a larger array of angles relative to the backbone than Hyflon. Probability density plots of side chain extension and angle are shown in Figure 6. The increase in flexibility of the 3M side chain allows for greater movement of the sulfonate group, facilitating the proton passing mechanism that shuttles protons between sulfonate potential wells.

A final interesting result from Figure 4 is the observation that Hyflon with a lower equivalent weight shows a higher diffusion constant than higher equivalent weight systems. These results are consistent with experiment, though the experimental dependence on equivalent weight is more pronounced than in our simulations.

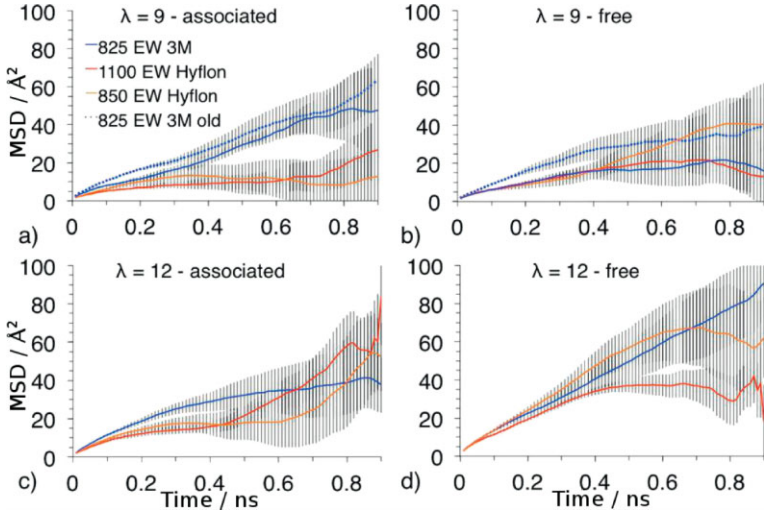

Fig. 5 MSD of protons associated with a sulfonate group and free from all sulfonate groups. The cutoff for determining association in this figure is 4.5 Å. Reprinted with permission from J. Savage, Y.-L. S. Tse, G. A. Voth, *J. Phys. Chem. C* 2014, *118*, 17436. Copyright 2014 American Chemical Society.

2.4 Morphology

Proton diffusion in PEMs is also highly dependent on morphology. Numerous PFSA membrane morphologies have been proposed, with no clear determination of which is most accurate. To compare the effects of membrane morphology, we present a study that investigated the structure and dynamics of Nafion systems constructed in different geometries [52].

In the study, we constructed morphologies with segregated hydrophobic and hydrophilic regions at several hydration levels and varied the size of the water layer. The two phase-segregated morphologies discussed here are lamellar and water channel models. In the lamellar case, the system consists of alternating slabs of hydrophobic and hydrophilic regions, the width of which is varied from 0.8 nm to 1.2 nm. The water channel model consists of cylindrical channels surrounded by the PEM; the radius of these water channels is varied from 1.0 nm to 1.2 nm. Representative snapshots of these morphologies are shown in Figure 7. In each case, the sulfonate groups collect at the hydrophobic-hydrophilic interface, as seen in Figure 3.

In the lamellar morphology, increasing the thickness of the water layer results in a decrease of the proton diffusion rate. Again, considering the majority of proton diffusion was initially thought to occur in the bulk-like water region of the membrane, this result runs counter to intuition. However, this result is in fact consistent with the mechanism proposed from the previous section. Consider the number of unique sulfonate groups visited by an individual excess proton. In lamellar systems where the height of the water layer is 1.0 nm, an excess proton is more likely to visit a large number of unique sulfonate

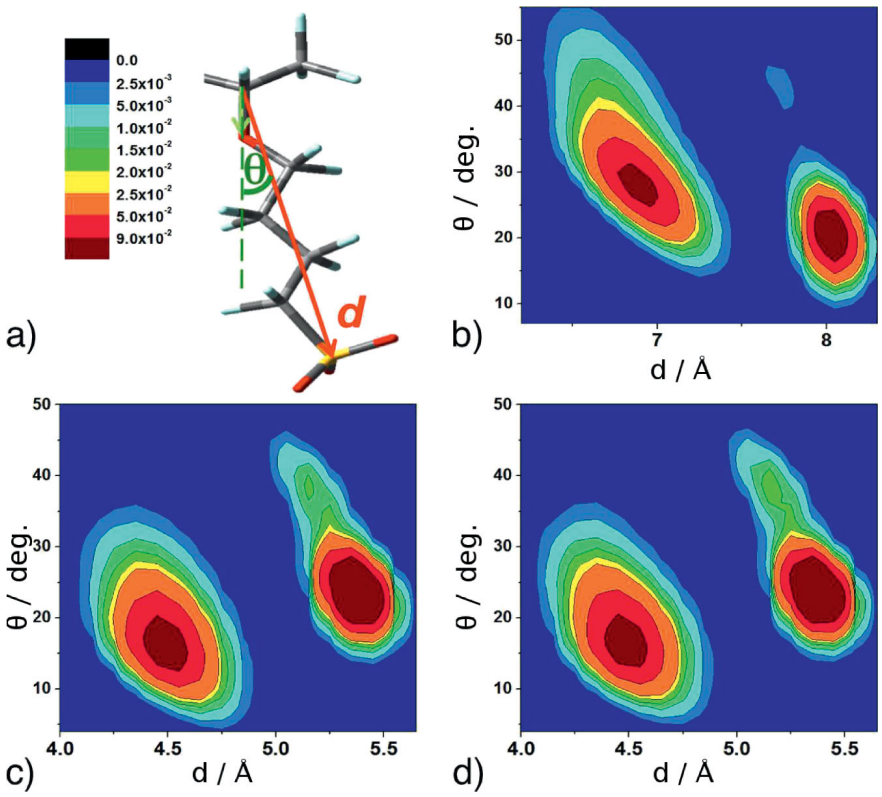

Fig. 6 (a) Definition of d and θ. Probability density distributions of d and θ for (b) 825 EW 3M, (c) 850 EW Hyflon, and (d) 1100 EW Hyflon. Reprinted with permission from J. Savage, Y.-L. S. Tse, G. A. Voth, *J. Phys. Chem. C* 2014, *118*, 17436. Copyright 2014 American Chemical Society.

groups than in systems where the height of the water layer is 1.2 nm. This behavior can be explained when considering the spatial density map of a proton, as shown in Figure 8. With a narrower water layer, the regions of high proton density are better connected than in systems with a thicker water layer. One would expect the thicker water layer to have higher proton diffusion, as there is a greater volume away from the Coulombic pull of the sulfonate groups. However, as seen in the S-CEC RDFs, and further illustrated in the density maps, a proton spends little time outside the second solvation shell, so the diffusion rate in such a region has a smaller contribution to the overall diffusion. More important for efficient transport is a large amount of overlap between the adjacent potential wells of sulfonate groups.

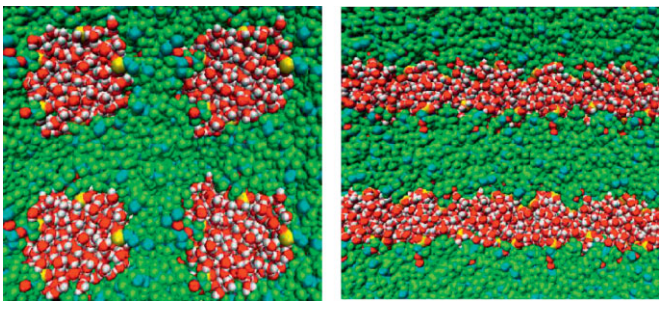

Fig. 7 Cross-sections of water channel model (left) and lamellar model (right). Reprinted with permission from S. Feng, J. Savage, G. A. Voth, *J. Phys. Chem. C* 2012, *116*, 19104. Copyright 2012 American Chemical Society.

In the water channel model, improved connectivity between regions preferred by protons again increases proton diffusion. In this morphology, protons actually diffuse more rapidly when the radius of the water channel increases. As before, excess protons infrequently visit the region near the center of the water pore, and the mobility is a function of connectivity between sulfonate groups. Figure 9 shows the S–S radial distribution function in the cylinder model for hydration levels 10 and 15 and channel radii of 1.0 nm and 1.2 nm. The height of the first peak, which represents the amount of sulfur atoms in the first solvation shell of other sulfur atoms, correlates well with proton diffusion rate.

3 Conclusions

We have summarized several recent simulation studies which use the (reactive) MS-EVB model to improve understanding of proton transport in PEMs. First, we have demonstrated the importance of the Grotthuss mechanism in overall proton transport by comparing the behavior of classical molecular dynamics to our MS-EVB model. While both reactive and classical studies underestimate the proton self-diffusion constant, MS-EVB shows that there is an anti-correlation of vehicular and Grotthuss components of the MSD, which has not been observed using nonreactive classical models.

We have then reviewed results comparing the effect of side chain length of the polymer to proton self-diffusion. This yielded a rather counterintuitive result: we found that increased side chain length and flexibility actually enhances proton transport. One might expect the Coulombic interaction between the hydronium ion and the charged sulfonate group would greatly hinder movement of the proton through the system. We find that this strong Coulombic interaction is actually not detrimental to proton self-diffusion as long as overlap between neighboring sulfonate potential wells is sufficiently large. We were then able to propose the primary mechanism for proton transport in PEMs involves their being passed between sulfonate groups, rather than diffusing freely in a bulk-water region like the center of a water pore. This proposed mechanism is further strengthened by the observation that protons spend very little time away from sulfonate groups, so that free diffusion cannot have a substantial contribution to the overall transport.

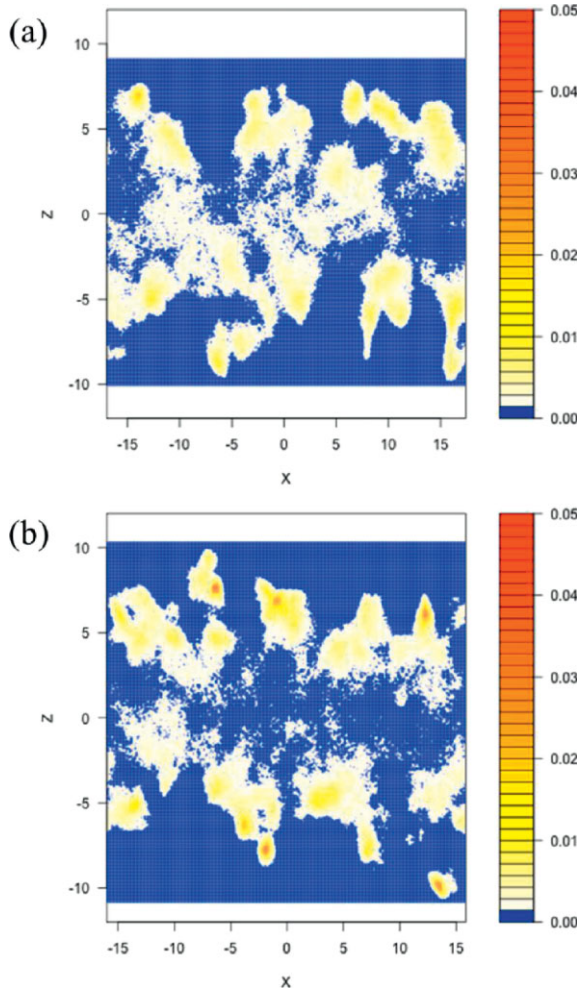

Fig. 8 Two-dimensional probability density of the excess proton in lamellar systems with an initial water layer width of (a) 1.0 nm and (b) 1.2 nm. Reprinted with permission from S. Feng, J. Savage, G. A. Voth, *J. Phys. Chem. C* 2012, *116*, 19104. Copyright 2012 American Chemical Society.

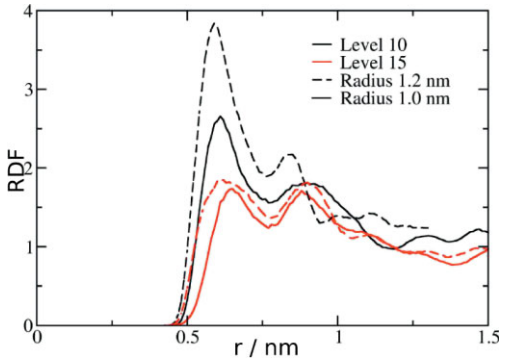

Fig. 9 Sulfur-sulfur RDF in the water channel morphology for hydration levels 10 and 15 for channel radii of 1.0 and 1.2 nm. RDF for hydration level 10 is shown in black; hydration level 15 in red; channel radius 1.0 nm in solid lines; and channel radius 1.2 nm in dashed lines. Reprinted with permission from S. Feng, J. Savage, G. A. Voth, *J. Phys. Chem. C* 2012, *116*, 19104. Copyright 2012 American Chemical Society.

Lastly, we used this proposed mechanism to compare the effects of morphology. We again see that increased aggregation of sulfonate groups enhances proton diffusion. In lamellar morphologies with water layers separating polymer layers, decreasing the thickness of the water layer improves proton mobility by increasing connectivity of sulfonates. In the water channel model, increasing the radius of the water channel has the same effect. These results suggest that morphology that maximizes overlap of sulfonate groups and side chains that maximize proximity of sulfonate groups can potentially improve fuel cell overall performance.

Notes

The authors declare no competing financial interests.

Acknowledgement

This research was supported by the Department of Energy (DOE), Office of Basic Energy Sciences (BES), Division of Chemical Sciences, Geosciences, and Biosciences, through Award No. DE-SC0005418.

References

[1] S. J. Hamrock, M. A. Yandrasits, *Proton Exchange Membranes for Fuel Cell Applications*, Vol. 46, Taylor & Francis, New York **2006**, pp. 219.
[2] C. Lixon Buquet, F. Hamonic, A. Saiter, E. Dargent, D. Langevin, Q. T. Nguyen, *Thermochim. Acta* **2010**, *509*, 18.
[3] K. Hongsirikarn, J. G. Goodwin Jr., S. Greenway, S. Creager, *J. Power Sources* **2010**, *195*, 7213.
[4] A. Kishi, M. Inoue, M. Umeda, *J. Phys. Chem. C* **2010**, *114*, 1110.
[5] I. M. Krivobokov, E. N. Gribov, A. G. Okunev, G. Spoto, V. N. Parmon, *Solid State Ionics* **2010**, *180*, 1694.
[6] J. Lu, S. Lu, S. P. Jiang, *Chem. Commun.* **2011**, *47*, 3216.
[7] B. R. Matos, E. I. Santiago, J. F. Q. Rey, A. S. Ferlauto, E. Traversa, M. Linardi, F. C. Fonseca, *J. Power Sources* **2011**, *196*, 1061.
[8] S. Mollá, V. Compañ, *J. Power Sources* **2011**, *196*, 2699.
[9] M. N. Silberstein, P. V. Pillai, M. C. Boyce, *Polymer* **2011**, *52*, 529.
[10] T. Sugawara, N. Kawashima, T. N. Murakami, *J. Power Sources* **2011**, *196*, 2615.
[11] C. Vogel, H. Komber, A. Quetschke, W. Butwilowski, A. Pötschke, K. Schlenstedt, J. Meier-Haack, *React. Funct. Polym.* **2011**, *71*, 828.
[12] M. Yoonessi, H. Heinz, T. D. Dang, Z. Bai, *Polymer* **2011**, *52*, 5615.

[13] Y. Zhao, Z. Jiang, L. Xiao, T. Xu, H. Wu, *J. Power Sources* **2011**, *196*, 6015.
[14] G. A. Giffin, G. M. Haugen, S. J. Hamrock, V. Di Noto, *J. Am. Chem. Soc.* **2012**, *135*, 822.
[15] M. Eikerling, S. J. Paddison, T. A. Zawodzinski, *J. New Mater. Electrochem. Syst.* **2002**, *5*, 15.
[16] S. S. Jang, V. Molinero, T. Cagin, W. A. Goddard, *J. Phys. Chem. B* **2004**, *108*, 3149.
[17] R. Paul, S. J. Paddison, *J. Phys. Chem. B* **2004**, *108*, 13231.
[18] S. J. Paddison, J. A. Elliott, *J. Phys. Chem. A* **2005**, *109*, 7583.
[19] R. Paul, S. J. Paddison, *J. Chem. Phys.* **2005**, *123*, 224704.
[20] M. K. Petersen, F. Wang, N. P. Blake, H. Metiu, G. A. Voth, *J. Phys. Chem. B* **2005**, *109*, 3727.
[21] M. K. Petersen, G. A. Voth, *J. Phys. Chem. B* **2006**, *110*, 18594.
[22] S. J. Paddison, J. A. Elliott, *Solid State Ionics* **2006**, *177*, 2385.
[23] S. J. Paddison, J. A. Elliott, *Phys. Chem. Chem. Phys.* **2006**, *8*, 2193.
[24] R. Devanathan, A. Venkatnathan, M. Dupuis, *J. Phys. Chem. B* **2007**, *111*, 13006.
[25] R. Devanathan, A. Venkatnathan, M. Dupuis, *J. Phys. Chem. B* **2007**, *111*, 8069.
[26] V.-A. Glezakou, M. Dupuis, C. J. Mundy, *Phys. Chem. Chem. Phys.* **2007**, *9*, 5752.
[27] A. Venkatnathan, R. Devanathan, M. Dupuis, *J. Phys. Chem. B* **2007**, *111*, 7234.
[28] M. K. Petersen, A. J. Hatt, G. A. Voth, *J. Phys. Chem. B* **2008**, *112*, 7754.
[29] S. Cui, J. Liu, M. E. Selvan, S. J. Paddison, D. J. Keffer, B. J. Edwards, *J. Phys. Chem. B* **2008**, *112*, 13273.
[30] I. H. Hristov, S. J. Paddison, R. Paul, *J. Phys. Chem. B* **2008**, *112*, 2937.
[31] R. Devanathan, A. Venkatnathan, R. Rousseau, M. Dupuis, T. Frigato, W. Gu, V. Helms, *J. Phys. Chem. B* **2010**, *114*, 13681.
[32] J. Yana, P. Nimmanpipug, S. Chirachanchai, R. Gosalawit, S. Dokmaisrijan, S. Vannarat, T. Vilaithong, V. S. Lee, *Polymer* **2010**, *51*, 4632.
[33] D. W. M. Hofmann, L. N. Kuleshova, B. D'Aguanno, *J. Power Sources* **2010**, *195*, 7743.
[34] Y.-K. Choe, E. Tsuchida, T. Ikeshoji, A. Ohira, K. Kidena, *J. Phys. Chem. B* **2010**, *114*, 2411.
[35] T. Ohkubo, K. Kidena, N. Takimoto, A. Ohira, *J. Mol. Model.* **2010**, *17*, 739.
[36] S. Ahadian, H. Mizuseki, Y. Kawazoe, *J. Membr. Sci.* **2011**, *369*, 339.
[37] G. Dorenbos, K. Morohoshi, *J. Chem. Phys.* **2011**, *134*.
[38] S. Ban, C. Huang, X.-Z. Yuan, H. Wang, *J. Phys. Chem. B* **2011**, *115*, 11352.
[39] M. H. Eikerling, P. Berg, *Soft Matter* **2011**, *7*, 5976.
[40] B. F. Habenicht, S. J. Paddison, *J. Phys. Chem. B* **2011**, *115*, 10826.
[41] A. I. Mehmet, S. Eckhard, *J. Phys.: Condens. Matter* **2011**, *23*, 234104.
[42] M. Esai Selvan, E. Calvo-Muñoz, D. J. Keffer, *J. Phys. Chem. B* **2011**, *115*, 3052.
[43] H. Abroshan, H. Akbarzadeh, F. Taherkhani, G. Parsafar, *Mol. Phys.* **2011**, *109*, 709.
[44] M. Phonyiem, S. Chaiwongwattana, C. Lao-ngam, K. Sagarik, *Phys. Chem. Chem. Phys.* **2011**, *13*, 10923.
[45] M. E. Selvan, D. J. Keffer, S. Cui, *J. Phys. Chem. C* **2011**, *115*, 18835.
[46] T. H. Yu, Y. Sha, W.-G. Liu, B. V. Merinov, P. Shirvanian, W. A. Goddard, *J. Am. Chem. Soc.* **2011**, *133*, 19857.
[47] S. Feng, G. A. Voth, *J. Phys. Chem. B* **2011**, *115*, 5903.
[48] J. A. Elliott, D. Wu, S. J. Paddison, R. B. Moore, *Soft Matter* **2011**, *7*, 6820.
[49] C. Wang, J. K. Clark, M. Kumar, S. J. Paddison, *Solid State Ionics* **2011**, *199*, 6.
[50] Q. Zhao, P. Majsztrik, J. Benziger, *J. Phys. Chem. B* **2011**, *115*, 2717.
[51] J. K. Clark, S. J. Paddison, M. Eikerling, M. Dupuis, T. A. Zawodzinski, *J. Phys. Chem. A* **2012**, *116*, 1801.
[52] S. Feng, J. Savage, G. A. Voth, *J. Phys. Chem. C* **2012**, *116*, 19104.
[53] Q. Wang, N. S. Suraweera, D. J. Keffer, S. Deng, J. Mays, *Macromolecules* **2012**, *45*, 6669.
[54] R. Jorn, G. A. Voth, *J. Phys. Chem. C* **2012**, *116*, 10476.
[55] R. Jorn, J. Savage, G. A. Voth, *Acc. Chem. Res.* **2012**, *45*, 2002.
[56] Y.-L. S. Tse, A. M. Herring, K. Kim, G. A. Voth, *J. Phys. Chem. C* **2013**, *117*, 8079.
[57] Q. F. Wang, D. J. Keffer, S. X. Deng, J. Mays, *J. Phys. Chem. C* **2013**, *117*, 4901.
[58] Q. F. Wang, D. J. Keffer, S. X. Deng, J. Mays, *Polymer* **2013**, *54*, 2299.
[59] J. Savage, G. A. Voth, *J. Phys. Chem. Lett.* **2014**, *5*, 3037.
[60] J. Savage, Y.-L. S. Tse, G. A. Voth, *J. Phys. Chem. C* **2014**, *118*, 17436.
[61] S. Liu, J. Savage, G. A. Voth, *J. Phys. Chem. C* **2015**, *119*, 1753.
[62] K. A. Mauritz, R. B. Moore, *Chem. Rev.* **2004**, *104*, 4535.
[63] K. D. Kreuer, M. Schuster, B. Obliers, O. Diat, U. Traub, A. Fuchs, U. Klock, S. J. Paddison, J. Maier, *J. Power Sources* **2008**, *178*, 499.
[64] M. Maalouf, B. Pyle, C.-N. Sun, D. Wu, S. J. Paddison, M. Schaberg, M. Emery, K. H. Lochhaas, S. J. Hamrock, H. Ghassemi, T. A. Zawodzinski, *ECS Trans.* **2009**, *25*, 1473.
[65] J. K. Clark, S. J. Paddison, *Solid State Ionics* **2012**, *213*, 83.
[66] A. P. Sunda, A. Venkatnathan, *J. Mater. Chem. A* **2013**, *1*, 557.
[67] X. Luo, S. Holdcroft, A. Mani, Y. Zhang, Z. Shi, *Phys. Chem. Chem. Phys.* **2011**, *13*, 18055.
[68] N. J. Economou, J. R. O'Dea, T. B. McConnaughy, S. K. Buratto, *RSC Adv.* **2013**, *3*, 19525.
[69] U. W. Schmitt, G. A. Voth, *J. Phys. Chem. B* **1998**, *102*, 5547.
[70] U. W. Schmitt, G. A. Voth, *J. Chem. Phys.* **1999**, *111*, 9361.

[71] T. J. F. Day, A. V. Soudackov, M. Cuma, U. W. Schmitt, G. A. Voth, *J. Chem. Phys.* **2002**, *117*, 5839.
[72] Y. Wu, H. Chen, F. Wang, F. Paesani, G. A. Voth, *J. Phys. Chem. B* **2008**, *112*, 467.
[73] C. J. T. Grotthuss, *Ann. Chim* **1806**, *58*, 54.
[74] M. K. Petersen, F. Wang, N. P. Blake, H. Metiu, G. A. Voth, *J. Phys. Chem. B* **2005**, *109*, 3727.
[75] F. Wang, G. A. Voth, *J. Chem. Phys.* **2005**, *122*, 144105.
[76] M. Levitt, M. Hirshberg, R. Sharon, K. E. Laidig, V. Daggett, *J. Phys. Chem. B* **1997**, *101*, 5051.
[77] Y. Wu, H. L. Tepper, G. A. Voth, *J. Chem. Phys.* **2006**, *124*, 024503.
[78] K. D. Kreuer, *J. Membr. Sci.* **2001**, *185*, 29.
[79] J.-C. Perrin, S. Lyonnard, F. Volino, *J. Phys. Chem. C* **2007**, *111*, 3393.
[80] S. Ochi, O. Kamishima, J. Mizusaki, J. Kawamura, *Solid State Ionics* **2009**, *180*, 580.

